

# Innovative remote plasma source for atomic layer deposition for GaN devices F

Cite as: J. Vac. Sci. Technol. A **39**, 062403 (2021); <https://doi.org/10.1116/6.0001318>

Submitted: 27 July 2021 . Accepted: 27 August 2021 . Published Online: 21 September 2021

 Harm C. M. Knoop,  Karsten Arts, Jan W. Buijter, et al.

## COLLECTIONS

Paper published as part of the special topic on [Atomic Layer Deposition \(ALD\)](#)

F This paper was selected as Featured



View Online



Export Citation



CrossMark

## ARTICLES YOU MAY BE INTERESTED IN

[Status and prospects of plasma-assisted atomic layer deposition](#)

Journal of Vacuum Science & Technology A **37**, 030902 (2019); <https://doi.org/10.1116/1.5088582>

[Overview of atomic layer etching in the semiconductor industry](#)

Journal of Vacuum Science & Technology A **33**, 020802 (2015); <https://doi.org/10.1116/1.4913379>

[Plasma-enhanced atomic layer deposition: Correlating O<sub>2</sub> plasma parameters and species to blister formation and conformal film growth](#)

Journal of Vacuum Science & Technology A **39**, 062402 (2021); <https://doi.org/10.1116/6.0001094>

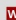
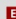
**HIDEN**  
ANALYTICAL

Instruments for **Advanced Science**

- Knowledge,
- Experience,
- Expertise

[Click to view our product catalogue](#)

Contact Hiden Analytical for further details:

 [www.HidenAnalytical.com](http://www.HidenAnalytical.com)  
 [info@hiden.co.uk](mailto:info@hiden.co.uk)



**Gas Analysis**

- ▶ dynamic measurement of reaction gas streams
- ▶ catalysis and thermal analysis
- ▶ molecular beam studies
- ▶ dissolved species probes
- ▶ fermentation, environmental and ecological studies



**Surface Science**

- ▶ UHVTPD
- ▶ SIMS
- ▶ end point detection in ion beam etch
- ▶ elemental imaging - surface mapping



**Plasma Diagnostics**

- ▶ plasma source characterization
- ▶ etch and deposition process reaction kinetic studies
- ▶ analysis of neutral and radical species



**Vacuum Analysis**

- ▶ partial pressure measurement and control of process gases
- ▶ reactive sputter process control
- ▶ vacuum diagnostics
- ▶ vacuum coating process monitoring








# Innovative remote plasma source for atomic layer deposition for GaN devices

Cite as: J. Vac. Sci. Technol. A 39, 062403 (2021); doi: 10.1116/6.0001318

Submitted: 27 July 2021 · Accepted: 27 August 2021 ·

Published Online: 21 September 2021



Harm C. M. Knoops,<sup>1,2,a)</sup>  Karsten Arts,<sup>2</sup>  Jan W. Buijter,<sup>2</sup> Luca Matteo Martini,<sup>2,b)</sup>  Richard Engeln,<sup>2</sup>   
Dilini Tania Hemakumara,<sup>1,3</sup> Michael Powell,<sup>1</sup> Wilhelmus M. M. (Erwin) Kessels,<sup>2,a)</sup>  Chris J. Hodson,<sup>1</sup>  
and Aileen O'Mahony<sup>1</sup>

## AFFILIATIONS

<sup>1</sup>Oxford Instruments Plasma Technology, North End, Bristol BS49 4AP, United Kingdom

<sup>2</sup>Department of Applied Physics, Eindhoven University of Technology, P.O. Box 513, 5600 MB Eindhoven, The Netherlands

<sup>3</sup>James Watt School of Engineering, University of Glasgow, Glasgow G12 8QQ, United Kingdom

**Note:** This paper is part of the 2022 Special Topic Collection on Atomic Layer Deposition (ALD).

**a) Authors to whom correspondence should be addressed:** [h.c.m.knoops@tue.nl](mailto:h.c.m.knoops@tue.nl) and [w.m.m.kessels@tue.nl](mailto:w.m.m.kessels@tue.nl)

**b) Present address:** Department of Physics, University of Trento, via Sommarive 14, I-38123 Trento, Italy.

## ABSTRACT

High-quality dielectric films could enable GaN normally off high-electron-mobility transistors (HEMTs). Plasma atomic layer deposition (ALD) is known to allow for controlled high-quality thin-film deposition, and in order to not exceed energy and flux levels leading to device damage, the plasma used should preferably be remote for many applications. This article outlines ion energy flux distribution functions and flux levels for a new remote plasma ALD system, Oxford Instruments Atomfab™, which includes an innovative, RF-driven, remote plasma source. The source design is optimized for ALD for GaN HEMTs for substrates up to 200 mm in diameter and allows for Al<sub>2</sub>O<sub>3</sub> ALD cycles of less than 1 s. Modest ion energies of <50 eV and very low ion flux levels of <10<sup>13</sup> cm<sup>-2</sup> s<sup>-1</sup> were found at low-damage conditions. The ion flux can be increased to the high 10<sup>14</sup> cm<sup>-2</sup> s<sup>-1</sup> range if desired for other applications. Using low-damage conditions, fast ALD saturation behavior and good uniformity were demonstrated for Al<sub>2</sub>O<sub>3</sub>. For films of 20 nm thickness, a breakdown voltage value of 8.9 MV/cm was obtained and the Al<sub>2</sub>O<sub>3</sub> films were demonstrated to be suitable for GaN HEMT devices where the combination with plasma pretreatment and postdeposition anneals resulted in the best device parameters.

© 2021 Author(s). All article content, except where otherwise noted, is licensed under a Creative Commons Attribution (CC BY) license (<http://creativecommons.org/licenses/by/4.0/>). <https://doi.org/10.1116/6.0001318>

## I. INTRODUCTION

GaN is an ideal material for power conversion and delivery, and within this field of power electronics, there is a strong drive to develop “E-mode” or “normally off” GaN high-electron-mobility transistors (HEMTs).<sup>1</sup> One of the prominent strategies to achieve such HEMTs is to use recess etching of the gate and to apply gate passivation by thin dielectric layers. Here, film and interface quality are essential, while at the same time, surfaces are sensitive to oxidation and damage. Al<sub>2</sub>O<sub>3</sub> is one of the materials commonly investigated as a dielectric for GaN HEMTs.<sup>2</sup> To deposit a high-quality Al<sub>2</sub>O<sub>3</sub> dielectric layer, plasma atomic layer deposition (ALD) could be a key solution. Plasma ALD has been demonstrated to be beneficial for GaN devices as plasma approaches enable high-quality film

growth and allow plasma pretreatment prior to film deposition. Furthermore, the self-limiting nature of ALD allows for conformal coverage of the gate recess by the gate dielectric, which holds also for plasma ALD.<sup>3</sup> To limit damage to the sensitive GaN surface, the plasma used should result in no or low damage. This can generally be achieved by using a remote plasma source.<sup>4</sup> However, up to now, low-damage remote plasma ALD has been difficult to do at large scale and at a sufficiently high rate to enable adoption for high-volume manufacturing applications.

This article discusses a new remote plasma ALD system, Oxford Instruments Atomfab™ [Fig. 1(a)], which includes an innovative, RF-driven, remote plasma source [Fig. 1(b)].<sup>5</sup> To investigate whether this source allows for low-damage processing, the plasma species have to be investigated. The energies and fluxes of

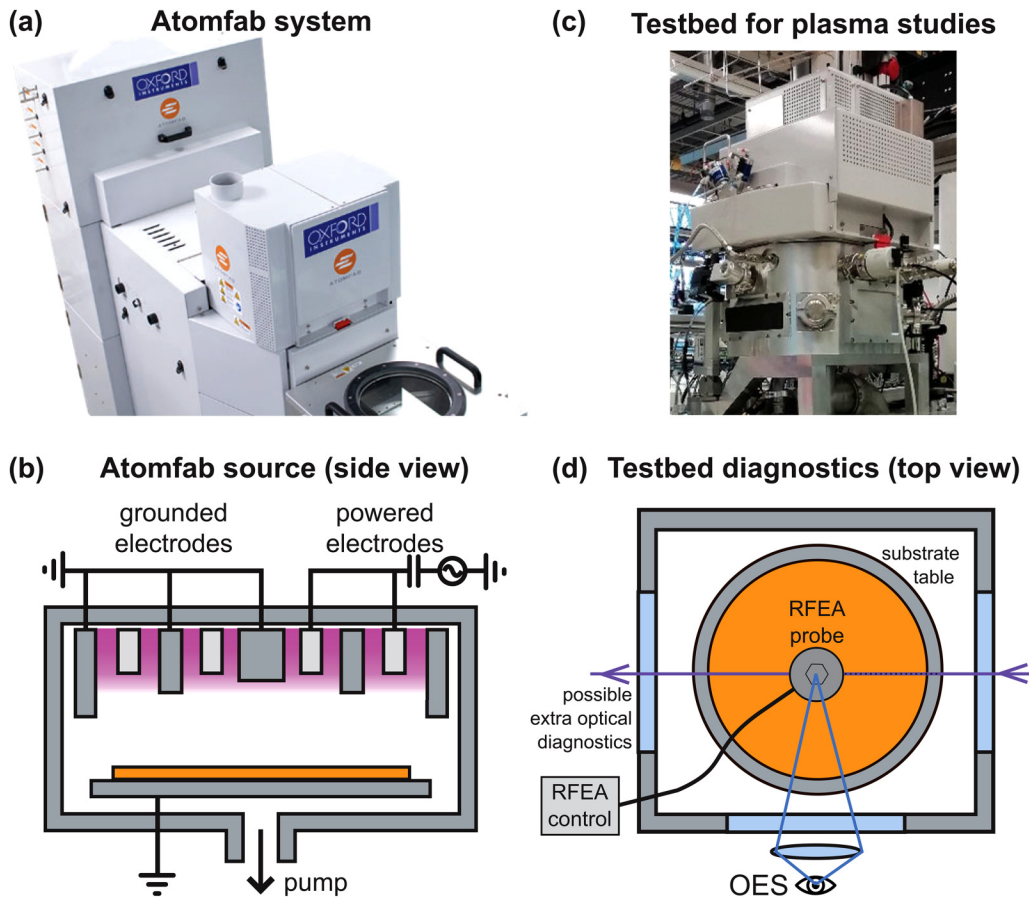


**FIG. 1.** Image of the Oxford Instruments Atomfab system (a) used in this work. A conceptual schematic (b) of the plasma source with powered (light gray) and grounded (dark gray) surfaces indicated. This plasma source was also put on a testbed system (c), which was used for the ion measurements and OES, the RFEA for probing the ion energy, and the flux was placed at the wafer level. Besides the RFEA, the testbed system was designed to allow for a range of optical diagnostics in the future (d).

certain species (namely, the ions, but also photons) have to be limited to avoid damage to device interfaces. Furthermore, in ALD, one would like to have high radical density to get high reactivity for fast saturation. In particular, the ion energy and flux values have to be compared to existing remote plasma ALD systems, e.g., those with inductively coupled plasma (ICP) sources.

Even though plasma parameters are important for the process and device results, there are only few reports of ion flux and energy under ALD conditions.<sup>6–9</sup> Also, the role of ions in plasma ALD has only recently seen an increase in reported studies.<sup>4,7,10,11</sup> Profijt *et al.* indicated that for ion flux density, the values are typically in the  $10^{13}$ – $10^{15}$   $\text{cm}^{-2} \text{s}^{-1}$  range for plasma ALD.<sup>12</sup> Due to the plasma sheath that develops at surfaces in contact with the plasma, the energy of ions impinging on the surface can be significant.<sup>12</sup> For plasma ALD, it is reported that ion energy values of <50 eV are generally present. For low-damage ALD on GaN surfaces, the plasma step in the ALD cycle probably would benefit from being in the low range of these flux and energy values. While it has been

reported several times that high-energy ions (e.g., >100 eV) can influence ALD processes,<sup>13–15</sup> it has recently been demonstrated that low-energy ions (e.g., <30 eV) can affect and also benefit plasma ALD.<sup>7,9</sup>

The total ion energy dose per ALD cycle has been identified as a key parameter,<sup>6,7</sup> which means that the product of ion energy and ion dose often determines the effect that ions have. Since the ion energy dose relates to both the ion flux and ion energy but also the used plasma exposure per ALD cycle, it is important to know the minimum plasma exposure time needed for saturated ALD growth. Ideally, the required plasma exposure is short with a low enough ion flux to limit the ion dose and at the same time with a high enough reactivity to allow for short cycle times and, therefore, high throughput. As we will show, when a remote plasma source allows very short saturation times for the plasma exposure, the ion energy dose can be minimal.

This article is structured as follows. First, the system is described with its key features. The plasma source is characterized

in terms of ion flux and ion energy values to assess whether these are in the regime suitable for low-damage processing and if this is also the case for the conditions needed for short cycle times. Precursor and plasma saturation and purge curves are obtained to confirm that ALD behavior is observed even with the short cycle time. This is accompanied with thickness and refractive index uniformity data and electrical properties. These results demonstrate indirectly that the plasma is intense enough to have short cycle time and achieve good uniformity and film quality. The paper is concluded by an analysis of the expected electrical properties for GaN HEMT devices at these fast cycle times.

## II. EXPERIMENT

Atomfab has been designed to be a remote plasma ALD system for high-volume manufacturing. It contains a plasma source in which RF power is capacitively coupled into the source using an automated matching unit. Powered and grounded counter electrodes form an electrode array above the grounded substrate surface. The grounded substrate is not part of the plasma generation zone due to the dimensioning of the powered and grounded parts of the array [Fig. 1(b), patent application PCT/GB2019/052763].<sup>5</sup> The source is designed to have the character of a remote plasma source although being close to the substrate (source to table distance  $\sim 6$  cm). It is compact to limit the effective chamber volume for rapid gas exchange (i.e., short residence time), and it is effective over the full 200 mm wafer diameter. The wafer-facing surfaces of the source are heated to avoid precursor and reaction product condensation. Operation occurs at a pressure of  $\sim 375$  mTorr unless otherwise stated. This pressure is between those typically used in ICP and capacitively coupled plasma systems, and it allows usage of industry-standard roughing pumps.

The typical plasma gas mixture used in the  $\text{Al}_2\text{O}_3$  process is an  $\text{O}_2/\text{Ar}$  gas mixture, and Ar is also used for the purging. This Ar purge flow is also present during the plasma step. The chamber gas mixture used here has a gas flow ratio of 3:2:2 being the ratio between plasma  $\text{O}_2$  gas, plasma Ar gas, and precursor purge Ar gas. Since Ar-diluted  $\text{O}_2$  plasmas are often referred to as  $\text{O}_2$  plasma, we will do the same here although it should be noted that changing Ar/ $\text{O}_2$  plasmas to pure  $\text{O}_2$  plasmas can significantly affect the plasma characteristics and hence also the film properties.<sup>8,16</sup> Plasma power usage is moderate and in the range of 100–300 W. In this work, 100 W is the standard operating power for the deposition experiments.

Besides an Atomfab system for deposition [Fig. 1(a)], an Atomfab plasma source testbed system was used in this work [Fig. 1(c)]. This testbed was designed for plasma studies such as ion analysis and optical emission spectroscopy (OES). The system uses the same plasma source and source to table distance. An Impedans Sesion Single retarding field energy analyzer (RFEA) is placed at the center of the grounded substrate table for the ion energy and flux measurements as shown in Fig. 1(d). To represent the distribution in ion flux as a function of ion energy, we will use the ion flux-energy distribution function (IFEDF) as also explained in a previous work.<sup>6</sup> In short, this distribution function indicates the distribution of ion energy for the ions reaching the substrate and the area below the distribution represents the ion flux. To

calculate ion flux from the probe current, we used the default factor of the SEMION software (which is  $860\,000\text{ m}^{-2}$ ), corresponding to an effective probe area of  $1.16 \times 10^{-6}\text{ m}^2$ .<sup>6,7</sup> For assessing the error in the ion flux, we have assumed a nonsystematic error of roughly 20%. This error is, for instance, caused by the effective collector area of the probe being dependent on the plasma pressure. Additionally, at high pressures, the relative uncertainty is higher since the signal to noise ratio is lower, which is also outside the specified pressure range of the RFEA of  $<300$  mTorr. To account for this uncertainty, we added as a base error level, the noise level. As an estimate of the noise level, we have used the IFEDF area below zero electron volts, which typically corresponds to an ion flux of  $\sim 5 \times 10^{12}\text{ cm}^{-2}\text{ s}^{-1}$ . Note that there is also a systematic error that can be roughly a factor two due to calibration uncertainties. This error is not accounted for in the error bars shown.  $E_{ion,max}$  is defined as the maximum energy, where the ion flux-energy distribution function is above the noise level (determined as  $\sim 10^{-3}\text{ nm}^{-2}\text{ s}^{-1}\text{ eV}^{-1}$ ). Note that even though an  $\text{O}_2/\text{Ar}$  mixture was used, the ions impinging on the surface are expected to be mostly the molecular ion  $\text{O}_2^+$  due to the reported rapid reactions of  $\text{Ar}^+$  via charge transfer with molecular  $\text{O}_2$ .<sup>10</sup> Pure Ar plasmas were used for comparison to see the effect of the gas composition on the ion flux and ion energy flux distribution (see the supplementary material).<sup>34</sup>

OES measurements were also carried out in the dedicated testbed system [Fig. 1(d)]. The light emitted by the plasma is collected through optical-grade UV fused silica windows by an off-axis UV-VIS parabolic mirror and focused into an optical fiber bundle. An Avantes multichannel spectrometer was used to record time-integrated emission spectra in the range between 200 and 1100 nm. Before each OES experiment, the plasma system was evacuated to a pressure lower than  $10^{-5}$  Torr by means of a turbomolecular pump to reduce background species levels.

Film depositions on blank silicon wafers and device test structures were performed on the Atomfab system at  $300^\circ\text{C}$ . Saturation curves and thickness and refractive index uniformity maps were obtained using a Woollam Alpha SE with a mapping station.

To assess the electrical performance, metal-oxide-semiconductor (MOS) capacitor structures for GaN on Si substrates were fabricated and characterized at the Glasgow University. The test structure fabrication flow and a schematic of the used device structure are available in the supplementary material.<sup>34</sup> Breakdown and capacitance-voltage (C-V) measurements were performed using a Keysight B1500A semiconductor parameter analyzer in conjunction with a microchamber probe station (Cascade Summit 12971B).

## III. RESULTS AND DISCUSSION

### A. Ion energy flux distribution and flux levels

The ion characteristics of the plasma source have been evaluated using the RFEA. To understand the behavior of the source and to obtain ion fluxes and ion energies that are easily measured, the standard pressure ( $\sim 375$  mTorr) is chosen as the maximum pressure in these experiments. The ion characteristics are shown in Figs. 2 and 3. Comparing these values to those from literature can be challenging as ion characteristics for ALD systems are not commonly available. In the discussion, we will use ion measurements

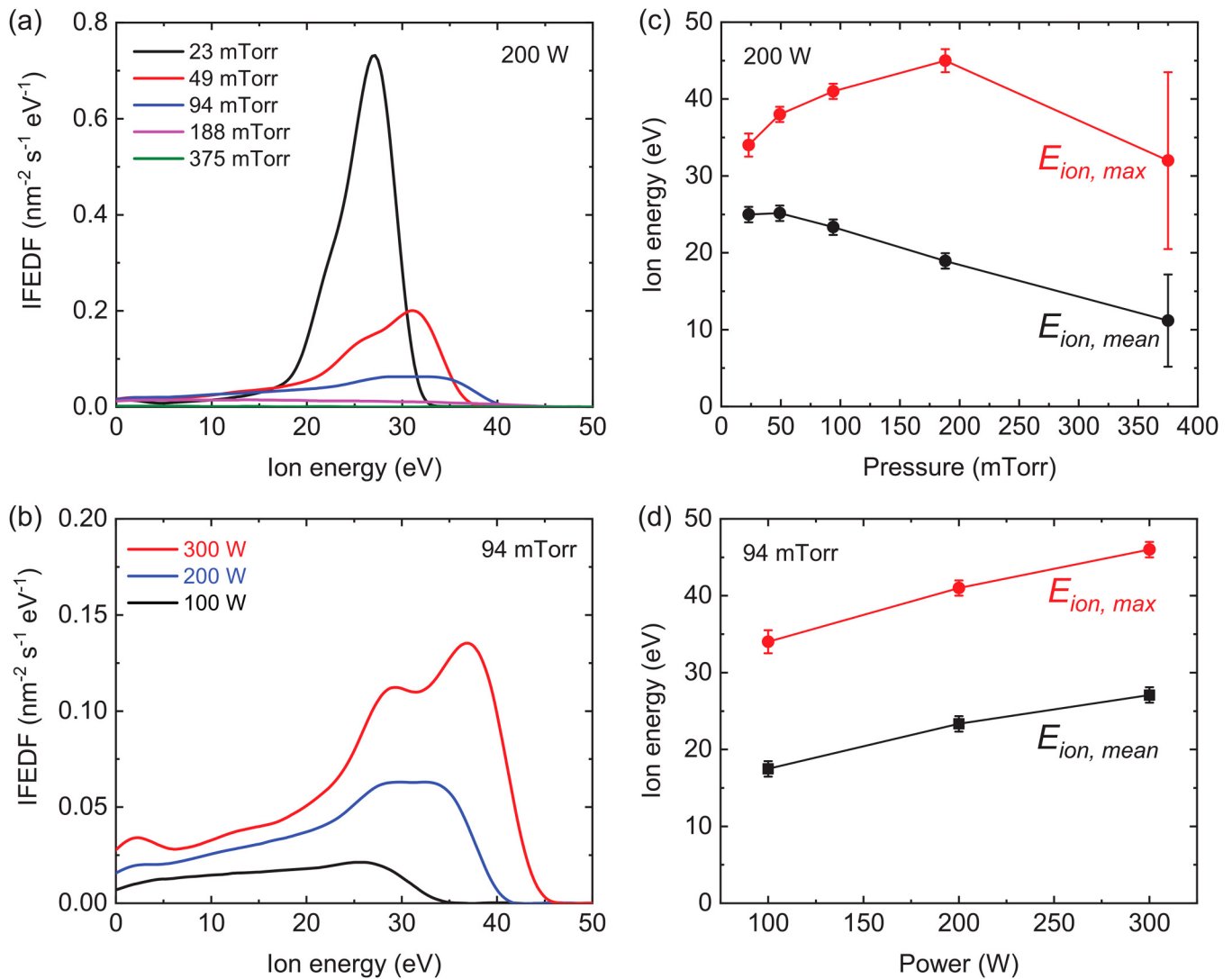


**FIG. 2.** IFEDFs for a range of chamber pressures for O<sub>2</sub> plasma at 200 W (a) and for a range of plasma powers for O<sub>2</sub> plasma at 94 mTorr (b). The average ion energy ( $E_{ion, mean}$ ) and the maximum ion energy ( $E_{ion, max}$ ) of the IFEDFs are plotted as a function of chamber pressure for O<sub>2</sub> plasma at 200 W (c) and as a function of plasma power for O<sub>2</sub> plasma at 94 mTorr (d). Note the values for the distribution at ~375 mTorr are close to the noise level of the RFEA, which leads to a larger error bar under this particular condition.

from previous work for a remote ICP system, FlexAL.<sup>6,17</sup> The FlexAL source is a remote ICP source and serves as an example of a remote plasma source used in plasma ALD, which is also known to allow for low-damage conditions.<sup>18</sup>

Figure 2(a) shows the IFEDFs for O<sub>2</sub> plasma at 200 W for a range of chamber pressures (see the supplementary material<sup>34</sup> for data on a logarithmic scale). The highest value for the ion flux, as indicated by the largest graph area for its distribution function, was achieved at the lowest pressure used of 23 mTorr. A strong reduction of the ion flux was observed when increasing the pressure as indicated by the decrease in the graph area for the curves. This

effect can be explained by a decreased plasma density as well as by enhanced ion-neutral collisions in the plasma sheath at higher pressures.<sup>17</sup> Figure 2(c) shows the average ion energy ( $E_{ion, mean}$ ) for these distribution curves of which the value generally decreases with pressure. Furthermore, the maximum ion energy ( $E_{ion, max}$ ) of the distribution is indicated, which increases as a function of pressure but decreases for the highest pressure measured. This general increase shows the broadening of the distribution, which indicates a likely increase in the plasma potential as the maximum kinetic energy of the ions reaching the substrate corresponds to the potential energy difference between the plasma potential and the

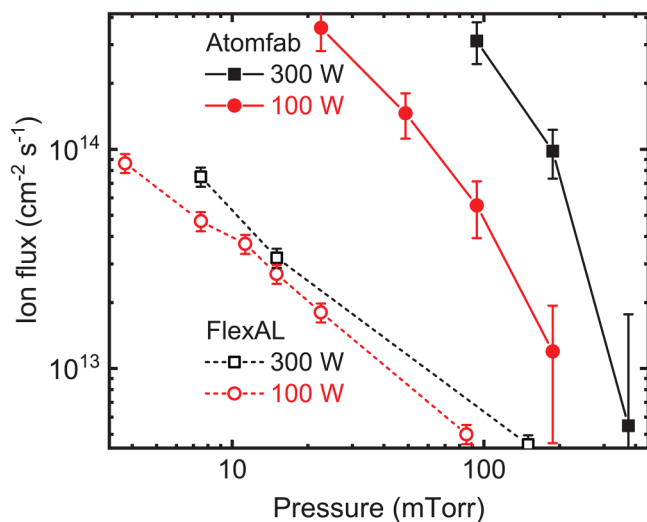


**FIG. 3.** Ion flux as a function of pressure for FlexAL and Atomfab sources for  $O_2$  plasmas of 100 and 300 W. Note that the results for FlexAL are taken from previous work and were obtained using an ion probe (Ref. 17). The results are plotted on a log-log scale for easy comparison. For the highest pressure value, the pressure is above the officially specified range of the RFEA ( $>300$  mTorr).

grounded substrate table. Such an increase in plasma potential was also observed by Zeuner *et al.* for increasing pressure and was related to a decrease in grounded area being in contact with the plasma.<sup>19,20</sup>

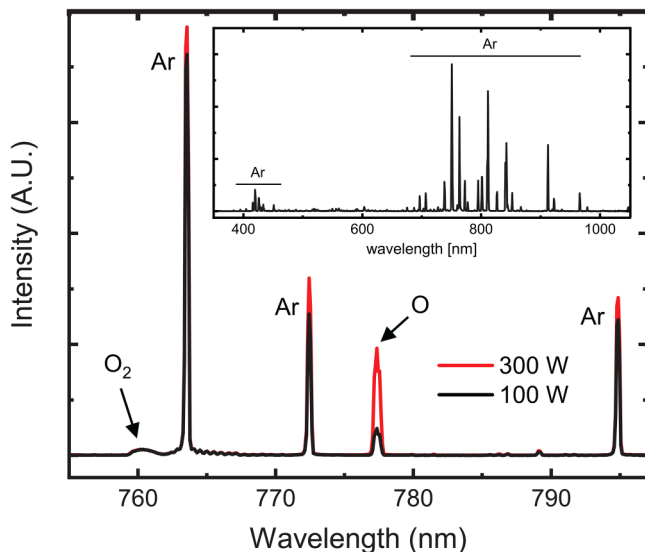


**FIG. 4.** Emission spectra for  $O_2$  plasma at 100 and 300 W power at  $\sim 375$  mTorr pressure. The emission recorded is mainly due to Ar (indicated over full range in the inset). The selected range in the main graph clearly shows emission from molecular and atomic oxygen as indicated.

Figure 2(b) shows the IFEDFs for a range of plasma powers for  $O_2$  plasma at a pressure of 94 mTorr (see the supplementary material<sup>34</sup> for data on a logarithmic scale). As expected, an increase of the ion flux was observed when increasing the power as indicated by the increase in the graph area of the distribution curves. Figure 2(d) shows the average ion energy ( $E_{ion,mean}$ ) as a function of plasma power for these IFEDFs, which generally increases with power. Furthermore, the maximum ion energy ( $E_{ion,max}$ ) of the distribution is indicated, which increases as a function of power similar to the average energy. This similar increase of both the average and maximum values agrees with the observation of the distribution becoming broader with especially an increase in ion flux density for higher energies. The same trends are observed for a pure Ar plasma (see the supplementary material).<sup>34</sup> Compared with literature values, the ion energies are in the same range as those reported for the standard operating range of ICP plasmas ( $<50$  eV).<sup>6</sup> A clear difference is the effect of plasma power on the ion energies. For ICP plasmas, this effect is generally minimal,<sup>6</sup> but for the Atomfab source, both  $E_{ion,mean}$  and  $E_{ion,max}$  scale with the plasma power. This could be explained by the capacitive coupling of the power, where capacitively coupled plasmas generally see an increase in ion energies with plasma power due to an increase in plasma potential and a reduction in plasma sheath thickness (due to an increase in plasma density) leading to less ion-neutral collisions.<sup>19</sup> Furthermore, in this source design, an increase in plasma power could make the plasma region larger and, therefore, less remote. Some features in the form of additional peaks visible in the IFEDF curves could be related to charge-exchange processes or originate from having a variety of ion species.<sup>19</sup>

Figure 3 shows a comparison of ion flux as a function of pressure for the Atomfab source and a FlexAL source (from the literature) for  $O_2$  plasmas at 100 and 300 W.<sup>17</sup> For both plasma powers indicated, a strong decrease in flux with pressure is observed for both Atomfab and FlexAL values as expected for a remote source. In spite of the relative proximity of the Atomfab plasma source to the substrate, similarly low ion flux values can be obtained with Atomfab as compared to ICP remote plasma (FlexAL), if Atomfab is operated above 100 mTorr. There is a stronger effect of plasma power on ion flux in Atomfab as compared to the remote ICP of the FlexAL, as visible by the larger difference between the 100 and 300 W curves. Regarding the standard processing conditions, the Atomfab plasma source at 100 W plasma power and  $\sim 375$  mTorr pressure gives modest ion energies ( $<50$  eV) and very low ion flux ( $<10^{13}$   $cm^{-2} s^{-1}$ ), similar to 50–100 mTorr conditions for the FlexAL ICP system.

The short plasma exposure time required for Atomfab to reach saturation ( $<0.25$  s of plasma) as demonstrated later, means that the ion energy dose per ALD cycle is relatively low ( $<1$  eV  $nm^{-1}$  cycle<sup>-1</sup>). For instance, for plasma ALD of  $SiO_2$ , it has been reported that such an ion energy dose leads to no observable effect of the ions and gives comparable results as to only having radicals present.<sup>7</sup> The determined low ion energy dose combined with the knowledge that only a short plasma exposure time is required for saturation suggests that this source can provide a high radical dose. Alternatively, the maximum ion flux in Atomfab is obtained at the lowest investigated plasma pressure and is approximately five times higher than the maximum flux obtained in the

used ICP system, which shows that a wide range of ion fluxes can be obtained if desired.

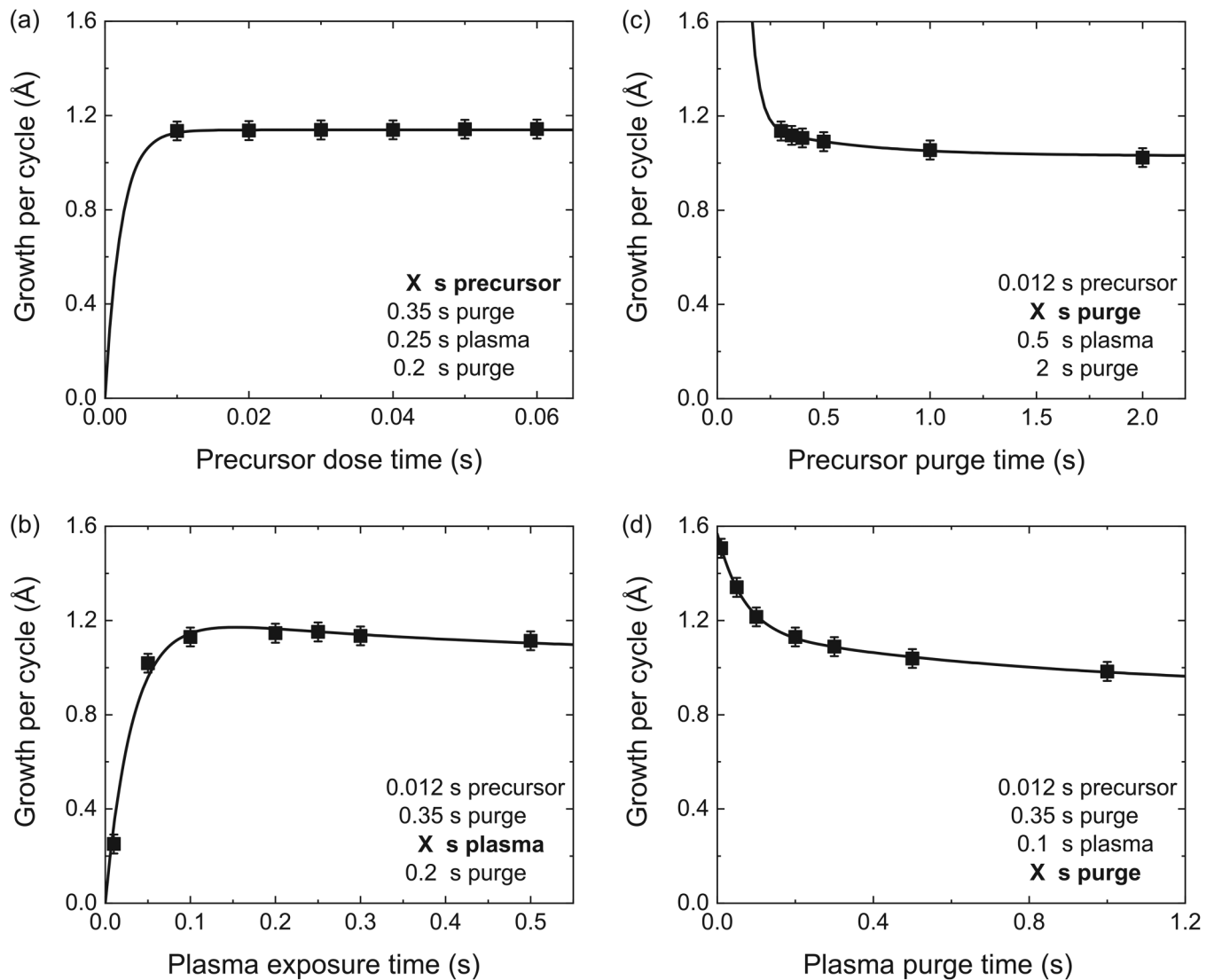
### B. Optical emission spectra

Figure 4 shows optical emission spectra collected above the substrate table surface for  $O_2$  plasma. The most prominent emissions observed were from Ar and O,<sup>21</sup> similar as observed in the literature for  $O_2/Ar$  plasma mixtures at these pressures.<sup>22</sup> Emission from the atmospheric absorption system (0,0) band of  $O_2$  is also visible and has been observed before in low pressure  $O_2$  plasmas.<sup>23,24</sup> With an increase in plasma power, the emission intensity increases, especially for the peak assigned to O radicals

suggesting a possible increase in O radical density. Furthermore, no emission for metal wall species such as Al was observed, which suggests no significant erosion of chamber and plasma source parts.

### C. Saturation curves and film uniformity

To assess whether the density of reactive plasma species is sufficient for fast processing at the chosen low-damage conditions, the ALD behavior was characterized by varying the ALD cycle time parameters. For these experiments, the standard conditions were at 300 °C and 100 W plasma power. Figures 5(a) and 5(b) show that fast saturation in the precursor and plasma dose times is obtained. Figures 5(c) and 5(d) show that the purge times needed for stable



**FIG. 5.** Growth per cycle for ALD of  $Al_2O_3$ . Data are given as a function of precursor (a) and plasma (b) dose times and the respective purge times (c) and (d) at 300 °C. Single and double exponential curve fits serve as a guide to the eye.

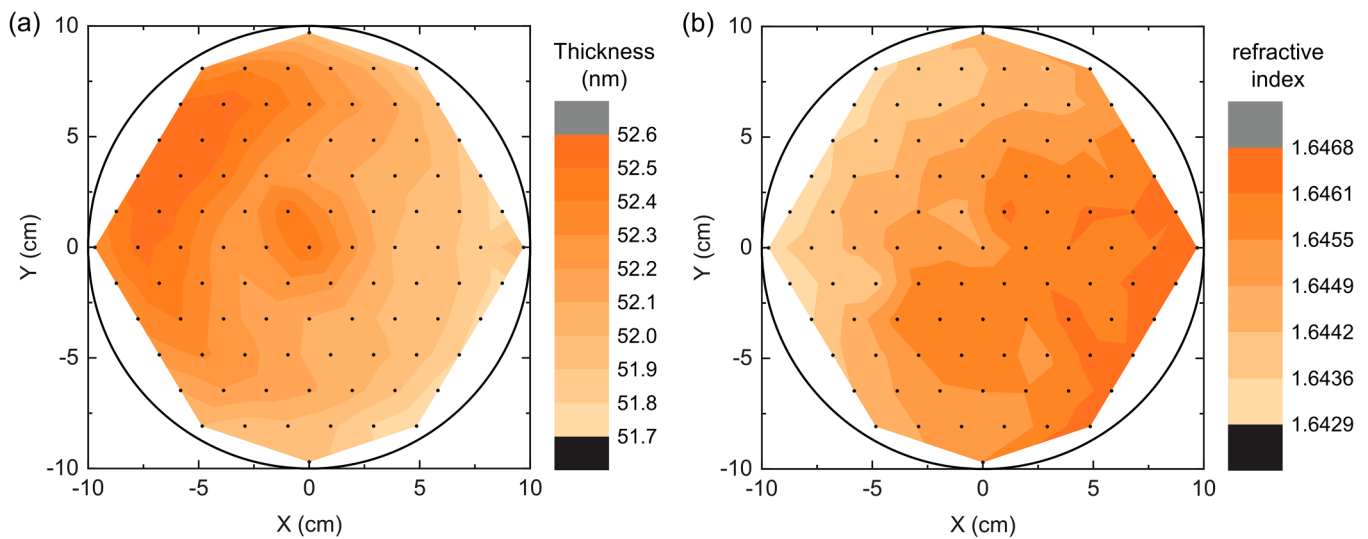


**FIG. 6.** Uniformity of the film thickness (a) and refractive index (b) for  $\text{Al}_2\text{O}_3$  over a 200 mm wafer using a <1 s cycle time at 300 °C. The data point locations are indicated. A film thickness nonuniformity  $\leq \pm 1.0\%$  and a refractive index ranging from 1.643 to 1.647 were achieved over the entire wafer surface.

growth per cycle (GPC) values are relatively short. Although precursor and plasma dose saturation times are important, only when combined with short purge times, do they allow us to achieve a short cycle time. Second, this saturation should be achieved over the entire wafer surface to allow for low nonuniformity of thickness and film properties. Here, using a <1 s cycle time, a film thickness nonuniformity  $\leq \pm 1.0\%$  was obtained as can be observed in Fig. 6 (a). This uniformity suggests ALD behavior over the wafer surface, which for remote plasma ALD systems generally requires at least 4 s cycle time.<sup>25</sup> In terms of film quality as indicated by the refractive index, a small spread in the obtained values was obtained over the entire wafer ranging from 1.643 to 1.647 [Fig. 6(b)]. Such short cycle times combined with low nonuniformity can be expected for direct plasma systems (due to the associated proximity of the plasma and the small reactor volume) but have not been reported to our knowledge for remote plasma systems. The saturated GPC values are similar to those reported in the literature for plasma ALD of  $\text{Al}_2\text{O}_3$  at 300 °C.<sup>26</sup>

#### D. Electrical data

To validate that these conditions were suitable for ALD of  $\text{Al}_2\text{O}_3$  on GaN HEMT devices, depositions were carried out using a standard Atomfab configuration. In addition to good electronic properties for the dielectric film, GaN HEMT devices also need a good interface between the dielectric and the GaN below. To achieve this, a low-damage plasma for surface pretreatment is desired. In the literature, some form of  $\text{H}_2$ ,  $\text{N}_2$ , or  $\text{NH}_3$  plasma treatment is often used.<sup>27–30</sup> In this work, we have chosen a 15 s, 100 W  $\text{NH}_3$  plasma at  $\sim 350$  mTorr as a demonstrator treatment. To assess the dielectric breakdown voltage, MOS capacitor structures for GaN on Si substrates were used. Figure 7 shows the voltage breakdown for a MOS capacitor structure for a 19.9 nm

$\text{Al}_2\text{O}_3$  film deposited at 300 °C with  $\text{NH}_3$  plasma pretreatment. A high breakdown voltage value of 8.9 MV/cm was obtained, which is very similar to other values reported in the literature for remote plasma ALD  $\text{Al}_2\text{O}_3$ .<sup>31</sup> The changes in the current density level before breakdown could be related to changes in related current conduction mechanisms (i.e., different tunneling emission processes),<sup>32</sup> but this discussion is outside the scope of this work.

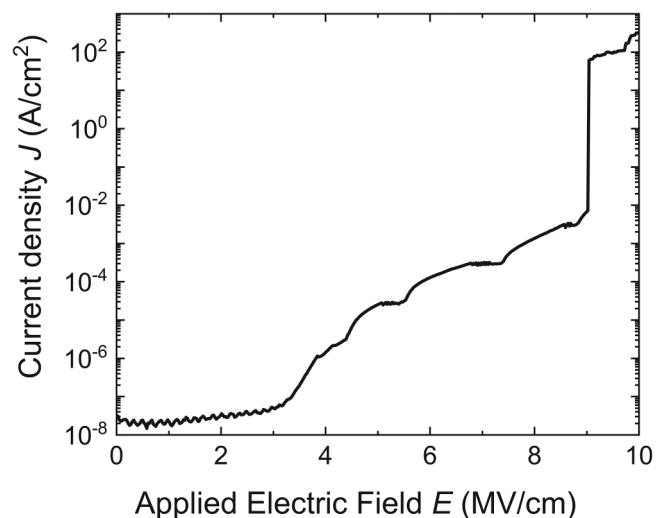


**FIG. 7.** Current density  $J$  as a function of the applied electric field  $E$  as deduced from the  $J$ - $V$  measurements over a 19.9 nm dielectric  $\text{Al}_2\text{O}_3$  film. Dielectric breakdown occurs at  $E_{bd} = 8.9$  MV/cm.



**TABLE I.** Effect of plasma pretreatment and FGA on hysteresis, dispersion, and leakage for Al<sub>2</sub>O<sub>3</sub> dielectric films at deposition temperature of 300 °C, a plasma pressure of ~375 mTorr, and a plasma power of 100 W. The typical uncertainty in hysteresis and dispersion values is indicated in the first row.

Pretreatment	FGA	Hysteresis (mV)	Dispersion (mV)	Leakage at 1 V (μA/cm <sup>2</sup> )
No	No	425 ± 25	425 ± 25	0.220
Yes	No	150	400	0.024
No	Yes	125	150	0.190
Yes	Yes	100	125	0.021

To further get insight into the suitability of these layers for GaN devices, Al<sub>2</sub>O<sub>3</sub> layers were grown on GaN HEMT test structures at 300 °C. The obtained capacitance-voltage curves are shown in the supplementary material.<sup>34</sup> Table I shows the key metrics from this analysis and compares the effect of plasma treatment on the hysteresis, the dispersion, and the leakage when using a plasma power of 100 W. We have also included the results after a 30-min forming gas anneal (FGA) at 430 °C, which is part of a typical process flow. As shown, the remote plasma Al<sub>2</sub>O<sub>3</sub> in the Atomfab combined with both an *in situ* pretreatment and an anneal produced devices with the best characteristics, indicative of an improved interface. Note that these results were achieved using a <1 s cycle time, while maintaining a high refractive index and film uniformity as plotted in Fig. 6. Both the pretreatment and FGA reduce the resulting hysteresis. The FGA affects mostly the dispersion values, and the pretreatment seems to be especially important to reduce the leakage current. Further optimization dedicated to a specific process flow and device structure should allow for further improvement. Note that a recent publication also demonstrated the low-damage nature of this plasma source for graphene-based devices.<sup>33</sup>

#### IV. SUMMARY AND CONCLUSIONS

A new low-damage remote plasma ALD system for high-volume manufacturing of Al<sub>2</sub>O<sub>3</sub> for GaN devices was evaluated, the Atomfab. The ion energy and flux values for the source were investigated and compared to those of a remote plasma inductively coupled plasma ALD system. Modest ion energies of <50 eV and very low ion flux values of <10<sup>13</sup> cm<sup>-2</sup> s<sup>-1</sup> were obtained at standard operating conditions suggestive of low-damage operation. The ion flux can be increased to the high 10<sup>14</sup> cm<sup>-2</sup> s<sup>-1</sup> range if desired for other applications. Saturation curves were determined, and saturation was confirmed for both dose and purge steps with a high uniformity in terms of film thickness and refractive index. The short plasma exposure time required for Atomfab to reach saturation (<0.25 s of plasma) means that the ion energy dose per ALD cycle is relatively low (<1 eV nm<sup>-1</sup> cycle<sup>-1</sup>). The low-damage nature was confirmed in GaN device representative tests. At these conditions, a breakdown voltage value of 8.9 MV/cm was obtained, which is very similar to other values reported in the literature for remote plasma ALD Al<sub>2</sub>O<sub>3</sub>. The combination with plasma pretreatments and forming gas anneal gave the best device metrics in terms of hysteresis, dispersion, and leakage.

#### ACKNOWLEDGMENTS

Some of this work is part of the research program HTSM with Project No. 15352, which received funding from the Netherlands Organization for Scientific Research (NWO). The authors would also like to thank J. J. A. Zeebregts, C. van Bommel, J. J. L. M. Meulendijks, and C. V. van Helvoirt for technical support.

#### DATA AVAILABILITY

The main data that support the findings of this study are available within the article and its supplementary material.<sup>34</sup> Ancillary data are available from the corresponding author upon reasonable request.

#### REFERENCES

- H. Amano *et al.*, *J. Phys. D: Appl. Phys.* **51**, 163001 (2018).
- Z. Yatabe, J. T. Asubar, and T. Hashizume, *J. Phys. D: Appl. Phys.* **49**, 393001 (2016).
- K. Arts, M. Utriainen, R. L. Puurunen, W. M. M. Kessels, and H. C. M. Knoops, *J. Phys. Chem. C* **123**, 27030 (2019).
- H. C. M. Knoops, T. Faraz, K. Arts, and W.M.M. Erwin Kessels, *J. Vac. Sci. Technol. A* **37**, 030902 (2019).
- G. Proudfoot, G. Waters, A. Peter, M. Cooke, and A. O'Mahony, Patent application PCT/GB2019/052763 (8 March 2020).
- T. Faraz, K. Arts, S. Karwal, H. C. M. Knoops, and W. M. M. Kessels, *Plasma Sources Sci. Technol.* **28**, 024002 (2019).
- K. Arts, J. H. Deijkers, T. Faraz, R. L. Puurunen, W. M. M. Kessels, and H. C. M. Knoops, *Appl. Phys. Lett.* **117**, 031602 (2020).
- D. R. Boris, V. D. Wheeler, J. R. Avila, S. B. Qadri, C. R. Eddy, and S. G. Walton, *J. Vac. Sci. Technol. A* **37**, 060909 (2019).
- K. Arts, H. Thepass, M. A. Verheijen, R. L. Puurunen, W. M. M. Kessels, and H. C. M. Knoops, *Chem. Mater.* **33**, 5002 (2021).
- D. R. Boris, V. D. Wheeler, N. Nepal, S. B. Qadri, S. G. Walton, and C. (Chip) R. Eddy, *J. Vac. Sci. Technol. A* **38**, 040801 (2020).
- C. Vallée *et al.*, *J. Vac. Sci. Technol. A* **38**, 033007 (2020).
- H. B. Profijt, S. E. Potts, W. M. M. Kessels, and M. C. M. Van de Sanden, *J. Vac. Sci. Technol. A* **29**, 050801 (2011).
- T. Faraz *et al.*, *ACS Appl. Mater. Interfaces* **10**, 13158 (2018).
- H. B. Profijt, M. C. M. van de Sanden, and W. M. M. Kessels, *Electrochem. Solid State Lett.* **15**, G1 (2011).
- H. B. Profijt, M. C. M. van de Sanden, and W. M. M. Kessels, *J. Vac. Sci. Technol. A* **31**, 01A106 (2013).
- J. R. Avila, S. B. Qadri, J. A. Freitas, N. Nepal, D. R. Boris, S. G. Walton, C. R. Eddy, and V. D. Wheeler, *Chem. Mater.* **31**, 3900 (2019).
- H. B. Profijt, P. Kudlacek, M. C. M. van de Sanden, and W. M. M. Kessels, *J. Electrochem. Soc.* **158**, G88 (2011).
- H. C. M. Knoops, T. Faraz, K. Arts, and W. M. M. Kessels, *J. Vac. Sci. Technol. A* **37**, 030902 (2019).
- M. Zeuner, H. Neumann, and J. Meichsner, *Jpn. J. Appl. Phys.* **36**, 4711 (1997).
- M. Zeuner and J. Meichsner, *Vacuum* **46**, 151 (1995).
- NIST, Atomic Spectra Database Standard Reference 78 (2020).
- Y. Wang, H. Qu, C. Zhang, and Q. Chen, *Sci. Rep.* **9**, 459 (2019).
- R. W. B. Pearse and A. G. Gaydon, *The Identification of Molecular Spectra* (Chapman and Hall, London, 1976).
- R. N. Peterson, L. L. Cogger, H. T. Meredith, and G. G. Shepherd, *Planet. Space Sci.* **27**, 1209 (1979).
- J. L. van Hemmen, S. B. S. Heil, J. H. Klootwijk, F. Roozeboom, C. J. Hodson, M. C. M. van de Sanden, and W. M. M. Kessels, *J. Electrochem. Soc.* **154**, G165 (2007).
- S. E. Potts and W. M. M. Kessels, *Coord. Chem. Rev.* **257**, 3254 (2013).

- <sup>27</sup>J. Son, V. Chobpattana, B. M. McSkimming, and S. Stemmer, *J. Vac. Sci. Technol. A* **33**, 020602 (2015).
- <sup>28</sup>S. Yang, Z. Tang, K.-Y. Wong, Y.-S. Lin, C. Liu, Y. Lu, S. Huang, and K. J. Chen, *IEEE Electron Device Lett.* **34**, 1497 (2013).
- <sup>29</sup>K. J. Chen, S. Yang, Z. Tang, S. Huang, Y. Lu, Q. Jiang, S. Liu, C. Liu, and B. Li, *Phys. Status Solidi A* **212**, 1059 (2015).
- <sup>30</sup>A. J. Kerr, E. Chagarov, S. Gu, T. Kaufman-Osborn, S. Madisetti, J. Wu, P. M. Asbeck, S. Oktyabrsky, and A. C. Kummel, *J. Chem. Phys.* **141**, 104702 (2014).
- <sup>31</sup>K. B. Jinesh, J. L. van Hemmen, M. C. M. van de Sanden, F. Roozeboom, J. H. Klootwijk, W. F. A. Besling, and W. M. M. Kessels, *J. Electrochem. Soc.* **158**, G21 (2011).
- <sup>32</sup>J. Yota, H. Shen, and R. Ramanathan, *J. Vac. Sci. Technol. A* **31**, 01A134 (2013).
- <sup>33</sup>B. Canto *et al.*, *Adv. Mater. Technol.* (published online) (2021).
- <sup>34</sup>See the supplementary material at <https://www.scitation.org/doi/suppl/10.1116/6.0001318> for the following: (i) IFEDFs for a range of chamber pressures and powers for O<sub>2</sub> plasma on a logarithmic scale, (ii) effect of plasma power on IFEDFs for Ar plasma and 53 mTorr, (iii) schematics and fabrication process flow of the used MOS capacitor structures, (iv) double-sweep C-V characteristics at 1 MHz of MOS capacitors after FGA, and (v) C-V characteristics of MOS capacitors after FGA at various frequencies from 1 kHz to 1 MHz.